ISTITUTO NAZIONALE DI FISICA NUCLEARE
Laboratori Nazionali di Frascati

LNF-84/19

S.Polizzi et al.: STRUCTURAL STUDY OF IRON AND CARBIDIC IRON BY SURFACE EXTENDED ENERGY LOSS SPECTROSCOPY

Estratto da:
Surface Science 136, 555 (1984)

Servizio Documentazione
dei Laboratori Nazionali di Frascati
Cas. Postale 13 - Frascati (Roma)

REPRINTED FROM

Surface Science

A JOURNAL DEVOTED TO THE PHYSICS AND CHEMISTRY OF INTERFACES

Volume 136, Nos. 2/3, 2 January 1984

STRUCTURAL STUDY OF IRON AND CARBIDIC IRON BY SURFACE EXTENDED ENERGY LOSS SPECTROSCOPY

S. POLIZZI * and F. ANTONANGELI

Gruppo PULS, Laboratori Nazionali di Frascati, Frascati, Italy

and

G. CHIARELLO and M. DE CRESCENZI

Dipartimento di Fisica, Universita della Calabria, Arcavacata di Rende, I-87036 Cosenza, Italy

pp. 555–570

NORTH-HOLLAND PUBLISHING COMPANY — AMSTERDAM

Surface Science 136 (1984) 555–570
North-Holland, Amsterdam

STRUCTURAL STUDY OF IRON AND CARBIDIC IRON BY SURFACE EXTENDED ENERGY LOSS SPECTROSCOPY

S. POLIZZI * and F. ANTONANGELI

Gruppo PULS, Laboratori Nazionali di Frascati, Frascati, Italy

and

G. CHIARELLO and M. DE CRESCENZI

Dipartimento di Fisica, Università della Calabria, Arcavacata di Rende, I-87036 Cosenza, Italy

Received 25 March 1983; accepted for publication 10 August 1983

We have applied the Extended Energy Loss Fine Structure (EELFS) technique for studying the radial distribution function of iron before and after the formation of a surface carbidic iron layer. The experiment is performed in the reflection mode with a conventional CMA electron analyzer. The energy range scanned is 50–500 eV. The Fourier analysis of the structures measured above the Fe $M_{2,3}$ edge and the C K edge gives structural information around different absorbing sites on surfaces which lack long range order. The structural results are compared with the local structure of bulk Fe_3C measured with the EXAFS technique. We have found that each carbon on the surface is coordinated to six nearest neighbours iron atoms in a trigonal prism coordination as in the crystalline iron carbide.

1. Introduction

One of the fundamental unknowns in surface physics still remains the exact determination of the atomic position in the lattice. At present, a number of experimental techniques are competitive for giving bond lengths, coordination numbers and vibration frequencies, both of clean surfaces and of chemisorbed atomic species [1]. Most surface structural techniques such as LEED [2] or ion back-scattering [3] can provide this kind of information but the fundamental requisite is that the system have long range order and even then the analysis is long, indirect and expensive.

The SEXAFS [4,5] (Surface Extended X-ray Absorption Fine Structure) technique seems to be the most promising tool to give a 3D structure around

* Present address: SISSA (Scuola Internazionale Superiore di Studi Avanzati), Strada Costiera Miramare, I-34100 Trieste, Italy.

each absorbing atom. Synchrotron radiation facilities, however, are not within the reach of every surface physics laboratory. Thus it is always of particular interest to develop and to refine electronic experimental methods that probe the local environment of surfaces.

We have recently demonstrated [6–8] that the radial distribution function $F(R)$ may be obtained from the analysis of the structures measured above the absorption edges in the reflection energy loss spectra. Experimentally the EELFS (Extended Energy Loss Fine Structure) technique is quite simple, requires little time of data collection with a conventional Auger apparatus and, moreover, it follows the theoretical basis and analysis procedure of EXAFS spectroscopy [9].

In this paper we have focussed our attention on the following points:
(i) sensitivity of EELFS spectroscopy to the surface as probed by the change of the local structure of bcc iron when a surface iron carbidic layer is formed;
(ii) assessment to which extent this technique provides the radial distribution function $F(R)$ in comparison to EXAFS. In particular, in this paper we compare the $F(R)$ obtained by EELFS analysis to the EXAFS $F(R)$ of a bulk Fe_3C above the Fe K edge.

We stress the possibility of the EELFS technique of obtaining $F(R)$ around different elements in the same compound. We have applied it to an interesting technological and catalytical problem like the interaction of carbon with the surface of iron.

2. Experimental and data collection

Pure polycrystalline Fe (Johnson–Matthey 99.99999%) was mechanically polished with a diamond paste and electrochemically etched before the insertion in the ultra-high-vacuum system.

The experimental Varian chamber, operating at $(1–2)\times 10^{-10}$ Torr, was equipped with an electron gun ($E_p = 10$ keV) coaxial to a single pass CMA (Cylindrical Mirror Analyzer), resolution $\Delta E/E = 0.4\%$, $I_{max} = 20\ \mu A$, according to the scheme of fig. 1.

The sample cleaning procedure consisted of alternate argon ion bombardment cycles followed by heating up to 700°C in order to remove surface contaminants, predominantly sulphur and phosphorus. In the final state the sample showed an Auger spectrum with the presence of no other components (well below 0.5%) than the elemental iron.

The carbidic iron layer was obtained by exposing at $T \leqslant 200$°C the clean iron, so prepared, to CO atmosphere – $(1–2)\times 10^{-6}$ Torr – for ~ 15 min. The Auger spectrum showed a surface composition close to an Fe_3C compound (inset of fig. 2). It is well known [10] that the CO dissociation occurs on clean transition metals (Ni, Co, Ru, Pt,...) at high temperature (100–300°C). On

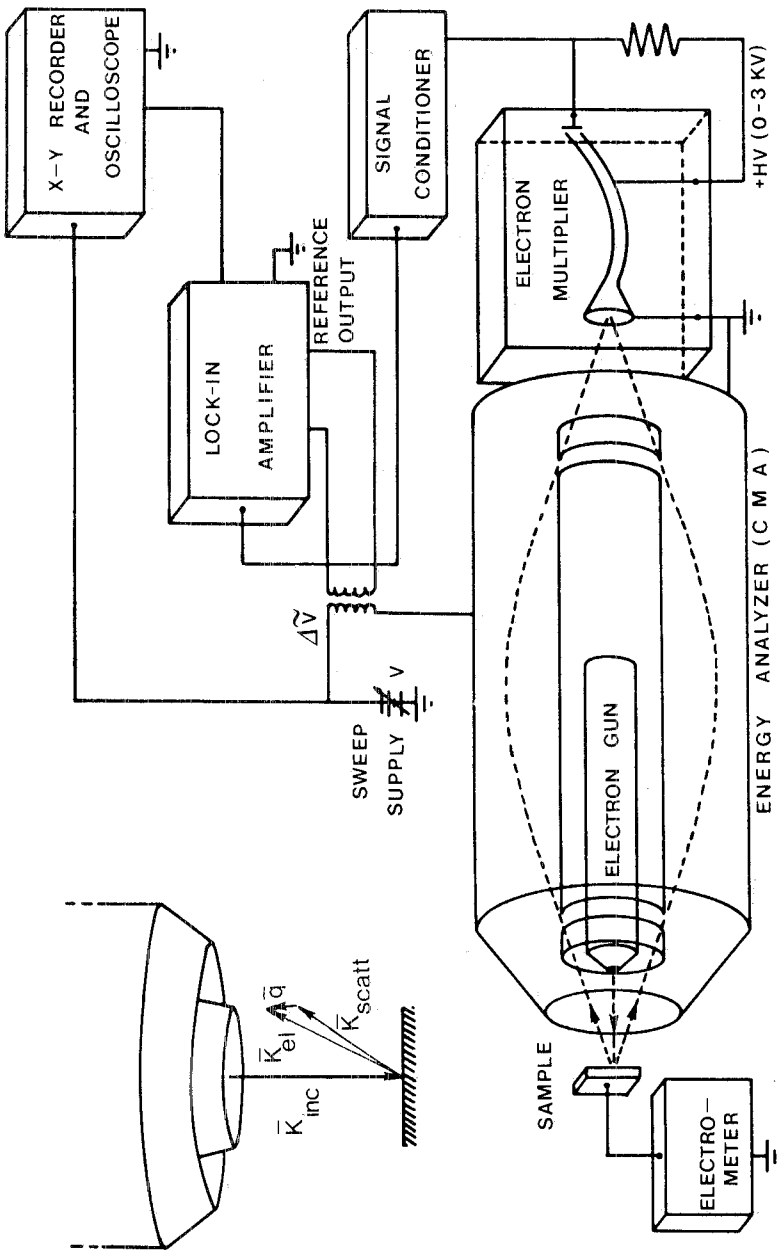

Fig. 1. Apparatus for measuring EELFS spectra. The electron gun is coaxial to the CMA and the primary beam impinges normally on the sample. A modulation of ~10 V must be applied to the outer cylinder of the analyzer. The K vector diagram is also shown.

iron, CO induces the formation of surface carbide according to the reaction:

$2\ CO \rightarrow$ superficial $C + CO_2$,

so that oxygen does not stick to the surface.

Fig. 2 shows electron loss spectra of Fe, recorded with a primary beam energy of 120 eV, before and after the formation of the iron carbidic layer. The spectra are displayed as a function of the second derivative of the electron yield $N(E)$ and a modulation of 1 V_{p-p} was used.

Fig. 3 shows the energy loss structures above the $M_{2,3}$ Fe core level collected with a primary beam energy of $E_p = 2000$ eV and a modulation of the outer cylinder of the CMA of ~ 10 V_{p-p}. This energy was chosen in order to maintain a surface sensitivity ($\lambda_{el} = 10$–15 Å), good instrumental resolution (compatible with our electron analyzer) and to avoid the superposition of Auger transitions. The collection data time was 15–20 min for each spectrum.

No electronic transitions due to pure iron are excited in the 100–400 eV energy loss region (the L_2 and L_3 levels occur at 708 and 721 eV, respectively)

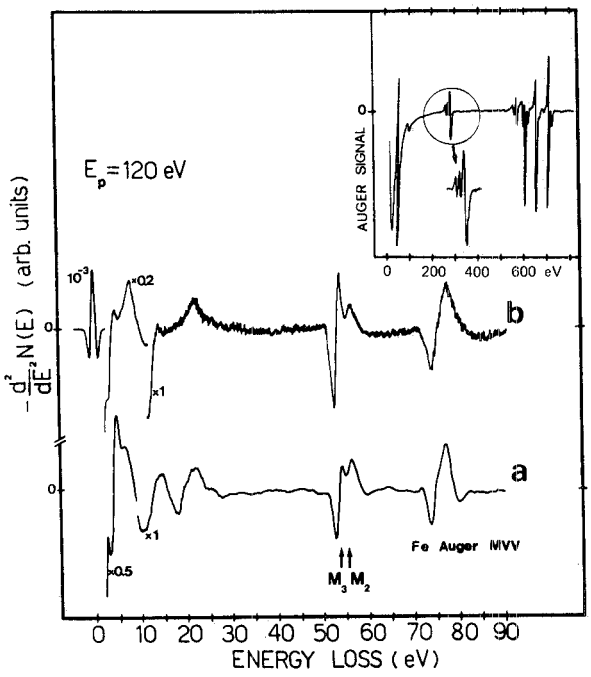

Fig. 2. Electron loss spectra, with $E_p = 120$ eV, of (a) clean Fe and of (b) the same sample after carbidization. The core levels $M_{2,3}$ and the Fe Auger spectrum are also shown. Inset: Auger spectrum of the carbidic iron layer.

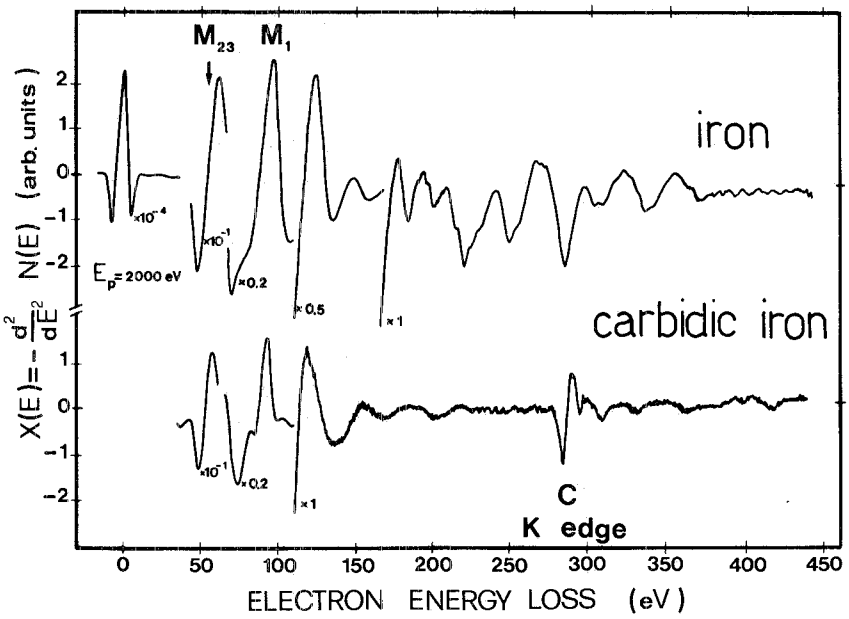

Fig. 3. Extended Energy Loss Fine Structure (EELFS) spectra of clean Fe before and after the formation of the iron carbide layer. The structures extend for about 300 eV above the $M_{2,3}$ core edge for clean Fe, while these structures, for the carbidic iron, are totally attenuated before the carbon K edge at ~ 285 eV, so that the Fourier analysis is possible around the two elements.

nor plasma replicas may be responsible for the structures of fig. 3. These structures do not change in intensity and shape by changing the primary beam energy (E_p = 1000–2000 eV) and furthermore they are not separated by a fixed amount of loss energies.

For these reasons these oscillations are called Extended Energy Loss Fine Structures (EELFS) [6] and we will show that from their analysis the structural distribution function may be obtained. For the case of the carbidic iron layer it is possible to measure not only EELFS osillations above the Fe $M_{2,3}$ core level but also structures related to the excitation of the carbon K edge (fig. 3) at ~ 285 eV, a region where the iron $M_{2,3}$ structures are completely attenuated.

3. Theoretical consideration

3.1. Analogies between EELFS and X-ray absorption

Inner shell electrons can be excited not only by the absorption of X-rays but also by the inelastic scattering of electrons, suggesting that the structural

information obtainable from X-rays (EXAFS spectroscopy) could be extracted also from electron excitation. However, since the two processes are basically different, the analysis of the relevant physical quantities involved is necessary.

In a reflection loss experiment one measures the scattering probability that an electron of energy E_p excites a transition in a medium, losing the corresponding energy ΔE and momentum q. This process is governed by the differential cross section [12,13]:

$$\frac{d^2N(E,q)}{dE\,dq} \propto -\frac{1}{q^3}\,\mathrm{Im}\frac{1}{\tilde{\varepsilon}_L(E,q)}, \tag{1}$$

where $\tilde{\varepsilon}_L(E,q) = \varepsilon_1 + i\varepsilon_2$ is the longitudinal dielectric function due to the peculiar character of the electron probe. The validity of eq. (1) has been discussed in ref. [14], where a careful comparison between optical and reflection EEL spectra of pure Fe is made in the 0–30 eV range. Here, we shall consider an inner level, where ε_2 is very low (10^{-2}–10^{-3} above 50 eV). In this case, using the standard approximation [11,15], eq. (1) reduces to:

$$\varepsilon_2 \sim \frac{d^2N(E,q)}{dE\,dq} \sim \frac{1}{q^3}|\langle\psi_f|e^{iq\cdot r_c}|\psi_i\rangle|^2\,\delta(E_f - E_i - \Delta E), \tag{2}$$

where $|\psi_f\rangle$ and $|\psi_i\rangle$ are the final and initial states of the excited core electron

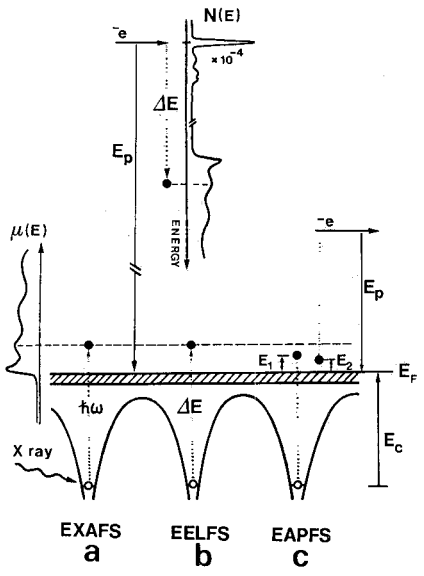

Fig. 4. Schematic picture of the excitations processes of (a) EXAFS spectroscopy, (b) EELFS and (c) EAPFS electronic spectroscopies.

and r_c is the core radius of the atom. The crucial point is that of assessing the limits in which eq. (2) approximates the one valid for optical absorption [9]:

$$\varepsilon_2 \sim |\langle \psi_f | \boldsymbol{e} \cdot \boldsymbol{r} | \psi_i \rangle|^2 \, \delta(E_f - E_i - \hbar\omega). \tag{3}$$

Schematic pictures of the electronic processes taking place in the excitation considered above are shown in figs. 4a and 4b, respectively. For small angle scattering, i.e. $qr_c \ll 1$, eq. (2) becomes:

$$\frac{d^2N(E,q)}{dE\,dq} \sim \frac{1}{q}|\langle \psi_f | \hat{\varepsilon}_q \cdot \boldsymbol{r}_c | \psi_i \rangle|^2 \, \delta(E_f - E_i - \Delta E), \tag{4}$$

where $\hat{\varepsilon}_q$ is the versor of the momentum transfer $\boldsymbol{q}$ and plays the same role as the electric field polarization $\boldsymbol{e}$. At energies much larger than the threshold energy of an inner shell, electrons can be considered nearly free and the scattering probability (contained in eq. (2)) peaks at a momentum transfer q, given by the conservation of energy and momentum, i.e.

$$\hbar^2 q^2 / 2m \simeq \Delta E - E_{edge} = \varepsilon; \tag{5}$$

q is so large that the dipole approximation (eq. (4)) should not be applicable.

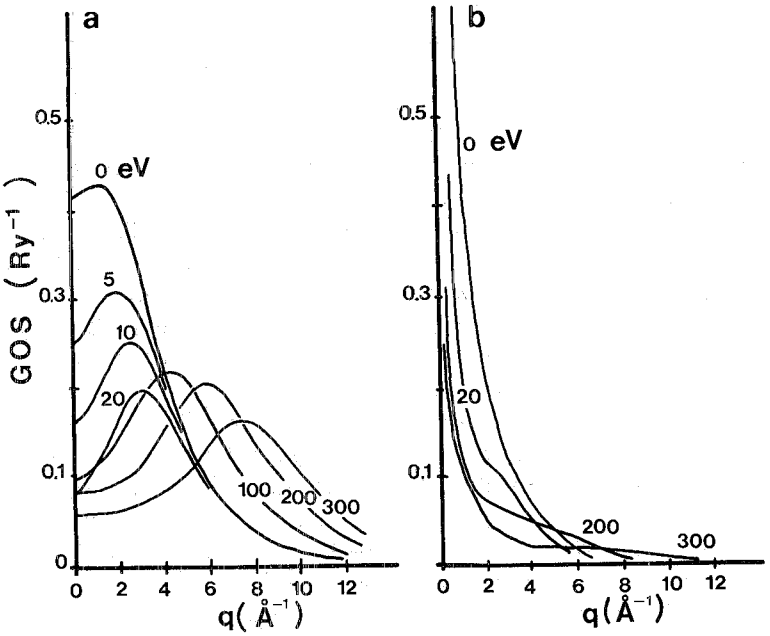

Fig. 5. (a) Generalized Oscillator Strengths (GOS) per unit energy in Ry (eq. (6)) for transitions into the continuum from the $M_{2,3}$ of Cu, as reported by Leapman, Rez and Mayers [15]. The continuum energies ε above the threshold are in eV. (b) GOS of (a) divided by the q dependence of eq. (2).

To clarify this point Leapman, Rez and Mayers [15] calculated the atomic Generalized Oscillator Strength (GOS):

$$\frac{df(E,q)}{dE} = \frac{1}{q^2}|\langle\psi_f|e^{iq\cdot r_c}|\psi_i\rangle|^2 \quad (6)$$

for K, L and M shells for transmission energy loss. We report in fig. 5a their calculation for the $M_{2,3}$ shell of Cu. The GOS is a continuum function of q peaking at a value given by eq. (5). This peak shifts towards high q values with increasing ε. This peak, called the "Bethe ridge" arises from the excitation of optically forbidden transitions. We stress that the GOS is finite even at $q \sim 0$ $Å^{-1}$ so that the $d^2N(E,q)/dEdq$ is large at low q values due to the $1/q$ dependence in eq. (2). The $d^2N(E,q)/dEdq$ function is reported in fig. 5b for the $M_{2,3}$ of Cu.

In every geometry where a given transferred momentum is collected, the measured cross section is proportional to the integral of eq. (2) between 0 and $q_{max} = (2m\Delta E)^{1/2}/\hbar$. Thus only the dipolar terms in the GOS ($q \ll 1$ $Å^{-1}$) are dominating.

On the basis of the above considerations, we expect a good correspondence between the reflection core edge losses and the photoabsorption spectra.

For energy losses higher than the absorption edge, the final continuum electronic state $|\psi_f\rangle$ must be constructed as an electronic plane wave that comes out from the excited atomic level and the backscattered part of this wave due to the presence of the neighbour atoms in the solid [16,17]. This interference "final state" process is called EXAFS (Extended X-ray Absorption Fine Structure). It was widely demonstrated how from its Fourier analysis it is possible to obtain reliable radial distribution functions $F(R)$ not only for bulk materials [9,10] but also for adsorbed atomic species on solid surfaces [4,5,18]. The possibility of choosing a well-defined absorbing adatom in $F(R)$ and measuring directly the distances of the surrounding atoms (both on ordered and on disordered matrix) is the great advantage of the Surface-EXAFS technique compared to diffraction techniques. Another important peculiarity is the relatively simple level of data manipulation.

Recent experiments [11,19] have demonstrated that Extended X-ray Edge Loss Fine Structures (EXELFS) may be measured and their structural results are similar to those obtained with the EXAFS technique. However, all these experiments are performed in transmission mode utilizing self-supported thin films (500–1000 Å or less [20]) and high electron beam energies (50–200 keV), so that surface structural information cannot be singled out.

The present EELFS study has the following and unique advantages:
- it is performed in the reflection model with the same instrumental set-up utilized for Auger spectroscopy,
- it contains surface information due to the possibility to select not only the core levels of the *substrate* but also the K edges of the *chemisorbed species*

[21–23] (C, N, O,...) and their evolution during, for instance, an oxidation or carbidization process.

3.2. Difference between EELFS and EAPFS

Appearance Potential Spectroscopy [24,25] measures electronic transitions from a core level as a function of the incident electron energy. Similarly to EELFS, this technique involves the utilization of an electron beam probe. It is of particular interest to underline the difference existing in these two excitation processes.

In the case of EELFS, the photoelectron final state is a *single* electron one, due to the great energy difference between the absorbing electron and the primary electron that loses energy (fig. 4b). In an Extended Appearance Potential Fine Structure (EAPFS) [25–27] experiment the observed oscillations are a *two*-dimensional event (fig. 4c). The inelastic electron yield, in fact, may be written as [25,26]:

$$\sigma_{\mathrm{EAPFS}}(E_\mathrm{p}) \sim \int_{E_\mathrm{F}}^{E} \mathrm{d}E_1 \int_{E_\mathrm{F}}^{E} \mathrm{d}E_2 \, |M_0|^2 \, N(E_1)\, N(E_2)\, \delta(E + E_n - E_1 - E_2), \qquad (7)$$

where E_1 is the final energy of the incident electron, E_2 the final energy of the core electron, $N(E_1)$ and $N(E_2)$ are densities of states and M_0 is a two-electron transition matrix element. So that above an absorption edge the total inelastic scattering probability will involve an integral, containing also the interference EXAFS process, over all the possible final states of the two electrons.

Despite this inconvenience, bulk [27] and surface [28] structural experiments have shown the wide capability of the EAPFS spectroscopy. However, arguments in favour of the EELFS technique are the difficulties of the EAPFS technique in finding the correct lattice parameters in a straightforward way [27,28] due, probably, to the lack of the dipole selection rule when the incoming electron plane wave transfers all its momentum to the electronic transition, and the diffraction problems originating from the variation with the primary beam energy of the diffraction (LEED) pattern.

4. Data analysis and results

4.1. Interband and atomic transitions

The 0–30 eV loss region, in fig. 2 is dominated by interband and collective excitations. In ref. [14] a general guideline for the interpretation of the reflection energy loss spectra is given and applied to the case of pure Fe. The main result, obtained from a careful comparison with optical spectra, was that all the peaks observed in an ELS spectrum correspond to longitudinal excitations that occur in connection with, but not at the same energy, as band to

band transitions. For carbidic iron we must note that all the structures appear broadened and reduced in intensity compared to those of clean Fe. This is due to the more complex geometrical structure originating by the introduction of carbon in the ordered bcc iron matrix. The peak at ~ 8 eV, not present in the clean Fe spectrum, may be interpreted as due to transitions from the 2p-hybridized carbon level below E_F.

The $M_{2,3}$ core levels of iron and carbidic iron (in the 50–60 energy loss region) result from a doublet, separated by 1.6 eV, that corresponds to $3p_{1/2}$ and $3p_{3/2}$ atomic transitions. The Fe $M_{2,3}$ edges are similar to those of other $M_{2,3}$ levels (Ti, Cr, Ni, etc.) [29] of transition metals and display the so-called Fano [30] "lineshape" due to the interference between localized atomic excitations ($3p \rightarrow E_F^{3d}$) and transitions from 3d to continuum states above E_F.

The spectra of fig. 2 give the second derivative of $N(E)$ so that the Fano lineshape is not immediately observed but could be obtained via a fit procedure. On the other hand we are particularly sensitive to the broadening of the structures.

Dietz et al. [31] find that the intensities of the two spin–orbit components are related to the width of the empty d-like band above E_F. The relative intensities of the carbidic iron $M_{2,3}$ lineshape appear reversed compared to those of Fe (fig. 2a). This suggests that the width of the empty d-like band in carbidic iron is narrower than that of clean iron.

The last structure between 70–80 eV is the MVV iron Auger transition. Of course this structure is not a genuine loss and does not move by changing the primary beam energy. The Auger $M_{2,3}$ spectrum is generally related to the filled valence density of states below E_F. The Auger carbidic iron lineshape broadens towards low kinetic energy compared to that of pure iron. We assign this widening to the thicker density of states due to the presence of the carbon 2p-hybridized levels at the bottom of the Fe band.

4.2. Extended fine structures

The structural information around each excited atom is obtained from the fine structure above the M_{23} edge of fig. 3, following the same procedure of the EXAFS spectra [9].

Experimental spectra, recorded as the second derivative of the electron yield $N(E)$ (defined as $X(E) = -d^2N(E)/dE^2$) are Fourier transformed after conversion to the k space (fig. 6a) by means of the formula:

$$\tilde{F}(R) = \int_{k_{min}}^{k_{max}} X(k)\, k^n\, W(k)\, e^{-2ikR}\, dk, \tag{8}$$

where k is the photoelectron wave vector

$$k\,(\text{Å}^{-1}) = \sqrt{0.263(E - E_0)\,\text{eV}}\,,$$

E_0 is the edge onset, $W(k)$ is a window function that avoids truncation effects

in the Fourier integral. $X(k)$ may be related to the solid arrangement in which the excited atom is embedded by the EXAFS $\chi(k)$ formula [16,17]:

$$\chi(k) = \sum_j \frac{N_j \, e^{-2\sigma_j^2 k^2}}{kR_j^2} e^{-2R_j/\lambda(k)} F_j(k,\pi) \sin\left[2kR_j + \phi_{tot}(k)\right], \tag{9}$$

where R_j is the atomic position from the absorber of the backscattered j atoms with amplitude $F(k,\pi)$ and coordination number N_j. Thermal vibrations and the photoelectronic mean free path $\lambda(k)$ are included in the two exponential functions.

The $\tilde{F}(R)$ obtained for the $M_{2,3}$ core edge of pure iron is shown in fig. 6b. All the observed structures in $\tilde{F}(R)$ are independent of the integration limits k_{max} and k_{min} and a reduced Δk interval produces only a broadening of the peaks. We note that, due to the second derivative of $N(E)$, the structures of the radial distribution function in eq. (7) are multiplied by $\sim R^2$.

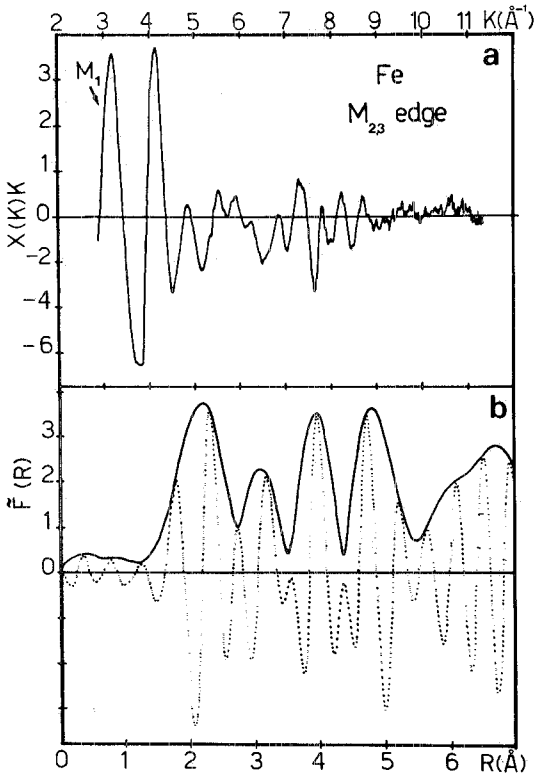

Fig. 6. (a) EELFS $X(k)k$ of clean Fe above the $M_{2,3}$ core edge. (b) Radial distribution function obtained via Fourier transform of the above spectra between $k_{min} = 3.3$ Å^{-1} and $k_{max} = 11.5$ Å^{-1}, so that the M_1 atomic contribution is not included in the analysis.

A comparison with published results, for Cu and Ni [6,7], shows that Fe has a more complex $M_{2,3}$ EELFS structure and this results in the $\tilde{F}(R)$ where more distant shells from the absorbing atom are distinguishable. This feature, already noted in the EXAFS analysis of Fe [32] (above the K edge), is related to the lower compactness of the Fe bcc lattice in comparison to the more closed packed structure of the fcc lattice.

We assign the first peak on fig. 6b, centred at 2.22 ± 0.03 Å, to the first neighbours atomic shell of Fe. This value must be properly corrected for the phase shift in order to coincide with the known crystallographic value of 2.48 Å [33].

Up to now only K and L edge phase shifts have been calculated [34] and tested experimentally. Recently, Ekardt and Tran Thoai [35] have computed the phase shifts for the $M_{2,3}$ edges of Cu and Ni. Their main result is that the use of the backscattering $L_{2,3}$ phase shift calculated by Teo and Lee is an acceptable approximation (within 0.05 Å in the position of $F(R)$) also for $M_{2,3}$ core levels.

Fig. 7 shows Teo and Lee's [34] total phase shifts for the K edge (dotted line) and $L_{2,3}$ (dashed line) for the Fe–Fe (absorber and backscatterer) pair. By correcting the position of the observed first peak in fig. 6b with the $L_{2,3}$ linear phase term, a 2.45 ± 0.05 Å first neighbour distance is obtained. The agreement with the known bulk value is fairly good in view of the uncertainty in the phase shift used and of possible relaxation effects in the lattice parameter of the first interatomic layer [36].

In contrast to the structures exhibited by the $\tilde{F}(R)$ of pure iron, the $\tilde{F}(R)$ of the iron carbide, above the $M_{2,3}$ Fe edge (fig. 8a), consists of only two peaks for $R \leqslant 5$ Å.

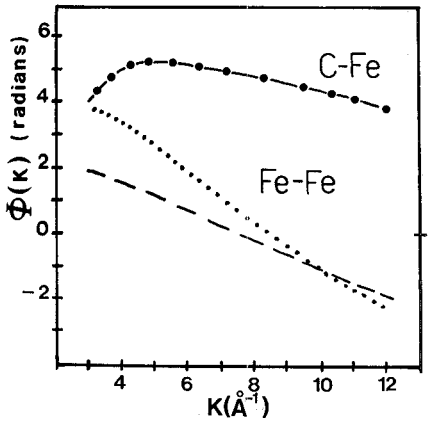

Fig. 7. Total phase shifts $\phi(k) = \phi(k)_{abs} + \phi(k)_{back} - \pi$ calculated by Teo and Lee [34]: (· · · · · ·) Fe–Fe pair for the K edge; (— — —) Fe–Fe for $L_{2,3}$ edges; (–·–·–) C–Fe phase for the K edge.

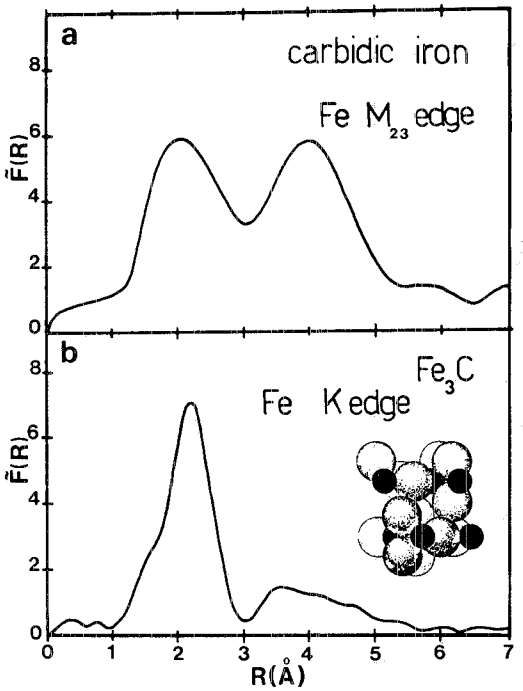

Fig. 8. (a) $\tilde{F}(R)$ as obtained from the EELFS above the Fe $M_{2,3}$ edge in iron carbide. The Fourier integral was extended up to 7.7 $Å^{-1}$. (b) $\tilde{F}(R)$ of bulk Fe_3C obtained around the Fe K edge with the EXAFS technique (2.5–13.5 $Å^{-1}$).

To better understand this lack of long range order, we have compared the $\tilde{F}(R)$ of the iron carbide with that measured in a bulk Fe_3C sample (fig. 8b), above the Fe K edge (7112 eV). The experiment was performed in transmission using the synchrotron radiation emitted by the Adone storage ring of the Frascati Laboratories, and the experimental set-up was described elsewhere [37].

The three non-equivalent iron positions around each iron site, due to the orthorhombic lattice geometry of Fe_3C [33] (inset of fig. 8b), lead to a complete absence of structures in $\tilde{F}(R)$ for $R \geqslant 5$ Å. In fact, a quasi-continuum distribution in R space of backscattering atoms strongly reduces the interference pattern for the outermost shells.

Fig. 9a shows the $\tilde{F}(R)$ obtained from the EELFS of the C K edge of the carbidic iron. Our present results for the function $\tilde{F}(R)$ show strong differences with the radial distribution function obtained for a graphite single crystal and for a graphitic monolayer of carbon grown on a Ni(111) surface studied with the same EELFS technique. Instead of two peaks in the $\tilde{F}(R)$ (at

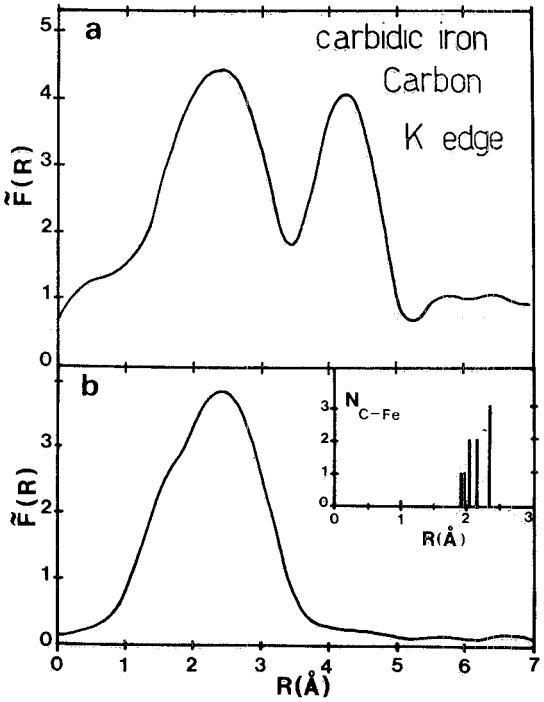

Fig. 9. (a) $\tilde{F}(R)$ obtained from the analysis of the EELFS spectrum of the carbidic iron layer around the C K edge. The Fourier analysis was extended between 2.0 and 7.5 $Å^{-1}$. (b) EXAFS model calculation $\tilde{F}(R)$ assuming (eq. (9)) the absorbing carbon to be bounded to the Fe atoms like in the iron carbide coordination (inset). The Fourier integration is performed with the same limits used for the experimental $\tilde{F}(R)$. Phase shifts (C–Fe) and backscattering amplitude (Fe) are taken from ref. [34].

~ 1 Å and 2 Å) related to the first and second neighbours in the graphite basal plane, the $\tilde{F}(R)$ of fig. 9a shows a broad asymmetric peak centred at 2.40 ± 0.03 Å. Fig. 9b shows the result of a theoretical EXAFS model for $\tilde{F}(R)$ including five backscattering Fe shells around each C atom, with coordination numbers and bond lengths of Fe_3C [33]. Phase shifts (C–Fe) and backscattering amplitude (Fe) are taken from ref. [34]. The model has been obtained by constructing the theoretical $\chi(E)$ of eq. (9). The second derivative of $\chi(E)$ was Fourier transformed using the same integration limits and the weight function used for the experimental results (2.0–7.5 $Å^{-1}$). An arbitrary change of the C–Fe distances (±0.05 Å) and coordination numbers gives a sizeable shift in the position of the maximum of the $\tilde{F}(R)$. The agreement between the theoretical model and the experimental EELFS $\tilde{F}(R)$ is quite good and confirms that the iron carbidic layer has structural properties which strongly

resemble those of the bulk iron carbide. Moreover it provides convincing evidence of the usefulness of our technique.

5. Conclusions

We have shown that structural surface properties may be obtained also from systems without long range order. This is obtained by analyzing EELFS oscillations measured in the reflection energy loss spectra above shallow core edges.

In the limits of the dipole approximation in the scattering cross section, the structural analysis follows the formalism and the procedure of the well established Surface-EXAFS technique [4,5,18].

We have investigated the geometry of a carbidic iron layer, starting from pure iron, around different elements (iron and carbon) and we have shown that the local environment around each carbon atom on the iron surface is similar to that of bulk iron carbide.

Acknowledgments

We would like to thank A. Balzarotti and M. Piacentini for discussions and for a critical reading of the manuscript. The technical help of F. Campolungo is also greatly appreciated.

References

[1] M.A. Van Hove, in: The Nature of the Surface Chemical Bond, Eds. TN. Rhodin and G. Ertl (North-Holland, Amsterdam, 1975) ch. 10.
[2] M.A. Van Hove and S.Y. Tong, Surface Crystallography by LEED (Springer, Berlin, 1979), and references therein;
P.M. Marcus, J.E. Demuth and D.E. Jepsen, Surface Sci. 53 (1975) 103.
[3] D.J. Godfrey and D.P. Woodruff, Surface Sci. 105 (1981) 438.
[4] P.H. Citrin, P. Eisenberger and R.C. Hewitt, Phys. Rev. Letters 41 (1978) 309.
[5] J. Stöhr, L. Johansson, I. Lindau and L. Pianetta, Phys. Rev. B20 (1979) 664.
[6] M. De Crescenzi, L. Papagno, G. Chiarello, R. Scarmozzino, E. Colavita, R. Rosei and S. Mobilio, Solid State Commun. 40 (1981) 613.
[7] L. Papagno, M. De Crescenzi, G. Chiarello, E. Colavita, R. Scarmozzino, L.S. Caputi and R. Rosei, Surface Sci. 117 (1982) 525.
[8] L. Papagno, L.S. Caputi, M. De Crescenzi and R. Rosei, Phys. Rev. B26 (1982) 2320.
[9] See: EXAFS Spectroscopy, Eds. B.K. Teo and D.C. Joy (Plenum, New York, 1981);
P.A. Lee, P.H. Citrin, P. Eisenberger and B.M. Kincaid, Rev. Mod. Phys. 53 (1981) 769.
[10] J.C. McCarty and R.J. Madix, Surface Sci. 54 (1976) 121;
J.C. Bertolini and B. Imelik, Surface Sci. 80 (1979) 586.
[11] J.J. Rusko, S.E. Schnatterly and P.C. Gibbons, Phys. Rev. Letters 32 (1974) 671.

[12] C.J. Powell and J.B. Swan, Phys. Rev. 115 (1959) 869.
[13] P.J. Feibelman, Surface Sci. 36 (1973) 558.
[14] E. Colavita, M. De Crescenzi, L. Papagno, R. Scarmozzino, L.S. Caputi, R. Rosei and E. Tosatti, Phys. Rev. B25 (1982) 2490.
[15] R.D. Leapman, P. Rez and D.F. Mayers, J. Chem. Phys. 72 (1980) 1232.
[16] P.A. Lee and G. Beni, Phys. Rev. B15 (1977) 2862.
[17] P.A. Lee and J.B. Pendry, Phys. Rev. B11 (1975) 2795.
[18] J. Stöhr, R. Jaeger and S. Brennan, Surface Sci. 117 (1982) 503.
[19] B.M. Kincaid, A.E. Meixner and P.M. Platzmann, Phys. Rev. Letters 40 (1978) 1296.
[20] P.E. Batson and A.J. Craven, Phys. Rev. Letters 42 (1979) 893.
[21] M. De Crescenzi, G. Chiarello, E. Colavita and R. Rosei, Solid State Commun. 44 (1982) 845.
[22] M. De Crescenzi, F. Antonangeli, C. Bellini and R. Rosei, Phys. Rev. Letters 50 (1983) 1949.
[23] R. Rosei, M. De Crescenzi, F. Sette, C. Quaresima, A. Savoia and P. Perfetti, Phys. Rev. B28 (1983) 1161.
[24] R.L. Park, J.E. Houston and D.G. Schreiner, Rev. Sci. Instr. 41 (1970) 1810;
R.L. Park and J.E. Houston, Surface Sci. 26 (1971) 664.
[25] G.E. Laramore, Phys. Rev. B18 (1978) 5254.
[26] T. Jack and T.H. Di Stefano, Phys. Rev. B19 (1979) 2831.
[27] P.I. Cohen, T.L. Einstein, W.T. Elam, Y. Fukud and R.L. Park, Appl. Surface Sci. 1 (1978) 538.
[28] M.L. den Boer, T.L. Einstein, W.T. Elam, R.L. Park, L.D. Roelofs and G.E. Laramore, Phys. Rev. Letters 44 (1980) 496;
M.L. den Boer, T.L. Einstein, W.T. Elam, R.L. Park, L.D. Roelofs and G.E. Laramore, J. Vacuum Sci. Technol. 17 (1980) 59.
[29] C. Kunz, in: Optical Properties of Solids; New Developments, Ed. B.O. Seraphin (North-Holland, Amsterdam, 1977) ch. 10.
[30] U. Fano, Phys. Rev. 124 (1961) 1866.
[31] R.E. Dietz, E.G. McRae and J. Weaver, Phys. Rev. B21 (1980) 2229.
[32] N. Motta, M. De Crescenzi and A. Balzarotti, Phys. Rev. B27 (1983) 4712.
[33] W.B. Pearson, Handbook of Lattice Spacing and Structure of Metals and Alloys (Pergamon, New York, 1958).
[34] B.K. Teo and P.A. Lee, J. Am. Chem. Soc. 101 (1979) 2815.
[35] W. Ekardt and D.B. Tran Thoai, Solid State Commun. 45 (1983) 1083.
[36] M. De Crescenzi, F. Antonangeli, C. Bellini and R. Rosei, Solid State Commun. 46 (1983) 875.
[37] S. Mobilio, F. Comin and L. Incoccia, Internal Report LNF 82-19/NT.